# System Design of a Novel Minimally Invasive Surgical Robot That Combines the Advantages of MIS Techniques and Robotic Technology

**HUAIFENG ZHANG**, **JIANMIN LI**, (Member, IEEE), **KANG KONG**, **AND SHUXIN WANG**, (Member, IEEE)

Key Laboratory of Mechanism Theory and Equipment Design of Ministry of Education, Tianjin University, Tianjin 300354, China

School of Mechanical Engineering, Tianjin University, Tianjin 300354, China

Corresponding authors: Jianmin Li (mjli@tju.edu.cn) and Kang Kong (kongkang103@tju.edu.cn)

**ABSTRACT** Existing minimally invasive surgical (MIS) robots are generally large, complex and expensive, which greatly increases the operation cost and limits the applications of MIS robot technology. To solve these problems, a small table-attached MIS robot that combines the high efficiency of the traditional MIS technique and the dexterity of robotic operations is proposed in this paper. The master and slave manipulators of the new robot are integrated, which allows the surgeon to manipulate the robot next to the operation table. Moreover, the novel design can be used with existing MIS instruments, providing surgeons dexterous operation and intuitive motion control with guaranteed operation efficiency. To simplify the structure of the robotic system, a multistage cable transmission structure is established. In addition, to reduce the difficulty of operations, especially suturing operations, a novel surgical instrument is developed with a "roll-pitch-distal roll" wrist and a quick-exchange interface. To overcome the uncoordinated hand-eye movement caused by the fulcrum effect, a motion mapping model is established for the robot. A prototype of the robot is developed and subsequently subjected to various tests. The results show that the instrument quick-exchange time is less than 20 s and that the maximum position and orientation trajectory errors are 0.46 mm and 0.87°, respectively. Finally, the feasibility and effectiveness of the proposed MIS robot are systematically verified through an in vivo animal experiment.

**INDEX TERMS** Animal experiment, cable transmission, MIS robot, motion mapping.

## I. INTRODUCTION

Currently, minimally invasive surgical (MIS) technology is generally accepted by both surgeons and patients. In minimally invasive surgery, several long thin surgical instruments are inserted into the patient's body through small incisions in the patient's body wall [1], [2]. Compared with invasive surgery, minimally invasive surgery provides several benefits, including less trauma, pain and blood loss, smaller scars, faster recovery times, considerably lower costs (due to shorter hospital stays), and reduced complication risks. However, surgeons require superior skills to perform MIS operations due to the following constraints caused by the incisions: (a) restricted instrumental degrees of freedom (DOFs), as only 4-DOF motions are allowed around the incisions [3]; (b) uncoordinated hand-eye movement, as the hand and the instrument tip exhibit opposite movement; and (c) low operating accuracy, as the surgeon's tremors are magnified at the end of the instrument. These constraints greatly limit the promotion and popularization of minimally invasive surgery.

With the development of robotic technologies and surgical technologies, the use of robots in minimally invasive surgery is rapidly increasing. The direct effects of robot-assisted MIS (RMIS) technology include (a) improved operation dexterity and precision, (b) restored natural hand-eye coordination, and (c) enhanced operation environment based on an ergonomic design. The introduction of three-dimensional vision technology has further promoted the development of robot-assisted minimally invasive surgery [4]. In recent years, MIS robots and related technologies have attracted increasing attention from researchers globally. Many prototypes have been successfully developed, including the da Vinci robot [5], [6], the MiroSurge robot [7], [8], the Avatera robot [9], the Revo-I robotic system [10]–[12], the Versius

The associate editor coordinating the review of this manuscript and approving it for publication was Jenny Mahoney.

robotic system [13], and the Senhance robot [14], [15]. These prototypes are master-slave robots, as the surgeon controls the remote slave manipulators by operating the master manipulators. Because the movements of the surgeon's hand are reproduced by the slave manipulators, these surgical robots can enable intuitive operation. Among the abovementioned prototypes, the da Vinci surgical robotic system, launched by Intuitive Surgical, is the most successful Food and Drug Administration (FDA)-approved commercial MIS robot [16]; this system has been well-received by the clinical community. However, because this robot requires a large operation room for the master and slave cart, a time-consuming setup procedure and high costs, the da Vinci surgical robotic system may not be the best choice for many surgical procedures and hospitals.

Miniaturization has become an important research direction in surgical robot technology. Rosen *et al.* [17] proposed a small, bendable surgical robot for single-portal minimally invasive surgery. Zemiti *et al.* [18] developed a compact, lightweight robot that is mounted directly on the patient's body. Kim *et al.* [19] designed a portable MIS robot with manipulation-sensing capability. Laribi *et al.* [20] proposed a spherical serial surgical robot that is compact, portable, and inexpensive. Li *et al.* [21] designed a compact, highly integrated MIS robot with master manipulators, slave manipulators, an image display device and a control system designed as a single unit. In addition, Choi and Park [22] developed a compact, modular telesurgical robot system that can simultaneously operate one laparoscopic arm and up to four instrument arms as needed. However, the simplified base and support structures may increase the difficulty and complexity of the preoperative setup procedure. Some handheld surgical robots have been developed to overcome the drawbacks of the large master-slave MIS robot. Matsuhira *et al.* [23] and Sieber *et al.* [24] proposed handheld surgical robots driven by electric motors. Hassan-Zahraee *et al.* [25] developed a lightweight robot with actuators that were separated from the main body. Miyazaki *et al.* [26] proposed a pneumatically driven handheld surgical robot. Sholev [27] and Awtar *et al.* [28] designed a compact handheld surgical robot with a wearable handle. Kim *et al.* [29] proposed a handheld surgical robot that hybridizes the tendon-gear mechanism and flexible tendon-sheath transmission. Payne *et al.* [30] devised a handheld mechatronic device with a flexible manipulator for arthroscopic interventions, and Yang *et al.* [31] developed a modular handheld surgical robot with interchangeable 4-DOF instruments. These handheld surgical robots are smaller in size and require less setup time. However, uncoordinated hand-eye movement remains a problem in minimally invasive surgery using these kinds of systems.

To create greater economic benefits for robot-assisted minimally invasive surgery, this paper proposes a new operation mode and presents the development of a compact surgical robot based on this operation mode. Existing operation modes are analyzed, and the new operation mode is elaborated. Then, an overview of the master-slave integrated surgical
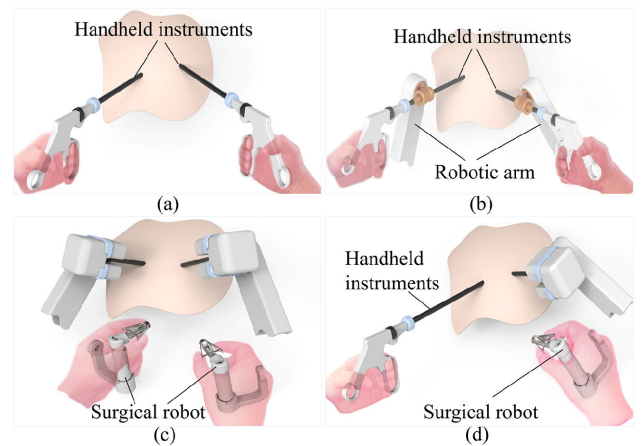


**FIGURE 1.** Comparison of different operation modes for minimally invasive surgery. (a) Handheld mode. (b) Robot-supported mode. (c) Robot-assisted mode. (d) Combined mode.

robot based on the proposed operation mode is presented. Furthermore, the transmission structure of the proposed robot is analyzed, and the motion mapping and control strategy are established based on the transmission modeling. An experimental study is implemented to validate the proposed surgical robot. Finally, a discussion is presented, and the conclusions are drawn.

## II. MATERIALS AND METHODS
### A. OPERATION MODE ANALYSIS
Existing operation modes for minimally invasive surgery mainly include (a) handheld mode, (b) robot-supported mode, and (c) robot-assisted mode. In surgery based on the first operation mode, the surgeon carries out the surgical procedures directly with handheld instruments, as shown in Fig. 1(a). Because of its simplicity, this operation mode has notably high efficiency. However, operation dexterity in this mode is limited, hand-eye coordination is poor, and tremors and fatigue caused by long-term operation will directly affect operation quality. For the second operation mode, such as that used in the $MC^2E$ system, a specially designed robot is used to support/hold the surgical instruments, which can help improve the operation accuracy and reduce the surgeon's fatigue, as shown in Fig. 1(b). However, the problem of hand-eye incoordination remains unsolved. The third operation mode, such as that used in the da Vinci surgical system, is generally master-slave operation, as shown in Fig. 1(c). The surgical robot, which is composed of several master and slave manipulators, provides more DOFs than the first two operation modes. However, such a system is usually complicated and requires a larger operating room, and the operation time is significantly extended, which reduces the operation efficiency.

In minimally invasive surgery, the instrument manipulated by the left hand is usually used to perform simple operations such as lifting, supporting and dragging, whereas the right instrument is used to perform complex or fine operations such as suturing, dissociation and cutting. Based on this division of labor, an operation mode that combines the advantages
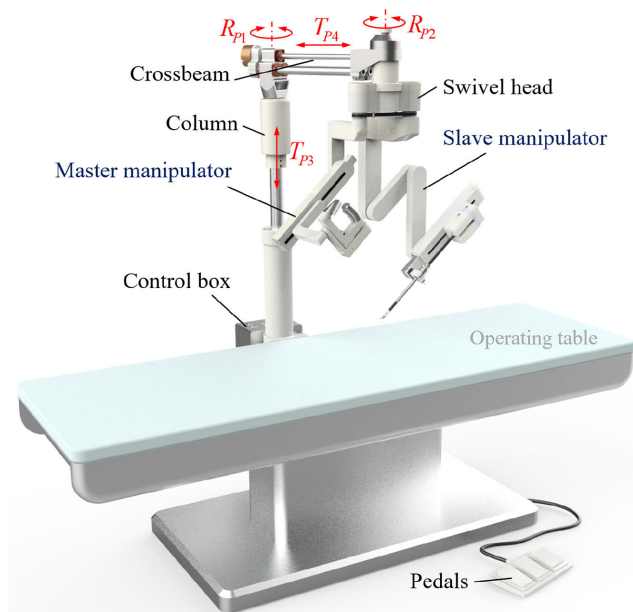
H. Zhang *et al.*: System Design of a Novel MIS Robot That Combines the Advantages of MIS Techniques and Robotic Technology

IEEE *Access*

**FIGURE 2.** Overall composition of the proposed master-slave integrated MIS robot.



**FIGURE 3.** Different body position requirements satisfied by rotating the swivel head.

of MIS techniques and robotic technology is adopted in this paper, as shown in Fig. 1(d). In this mode, a surgeon controls conventional instruments with their left hand and a specially designed new surgical robot with their right hand to perform surgery. By combining the two MIS technologies, the high efficiency and high precision requirements of MIS operation can be achieved. In addition, the size and weight of the robot can be significantly reduced. Thus, the portability of the robot is enhanced. Moreover, contact between the surgeon and the patient, which is lost in other robot-assisted operation modes, is preserved under the proposed operation mode, and interaction between the surgeon and the assistants can also be greatly improved. Then, to match the proposed operation mode, a novel master-slave integrated MIS robot is developed, the design details of which are described below.

### B. OVERVIEW OF THE ROBOT

As outlined above, a novel MIS robot is designed that a surgeon can operate in the proposed mode. During surgery, the surgeon manipulates the traditional MIS instruments with their left hand and operates the handle of the robot with their right hand; the operation is carried out under the guidance of a 3D image system. Therefore, the composition of the surgical robot requires only one master manipulator and one corresponding slave manipulator in this operation mode. The designed novel integrated master-slave MIS robot is shown in Fig. 2. The proposed surgical robot consists of one master manipulator, one slave manipulator, one control box, and a set of pedals. These structural units are highly integrated into one base mounted on an operating table. The base, which consists of a column and a crossbeam, can provide 4-DOF passive movements (rotations $R_{P1}$ and $R_{P2}$, and translations $T_{P3}$ and $T_{P4}$) for preoperative position adjustment of
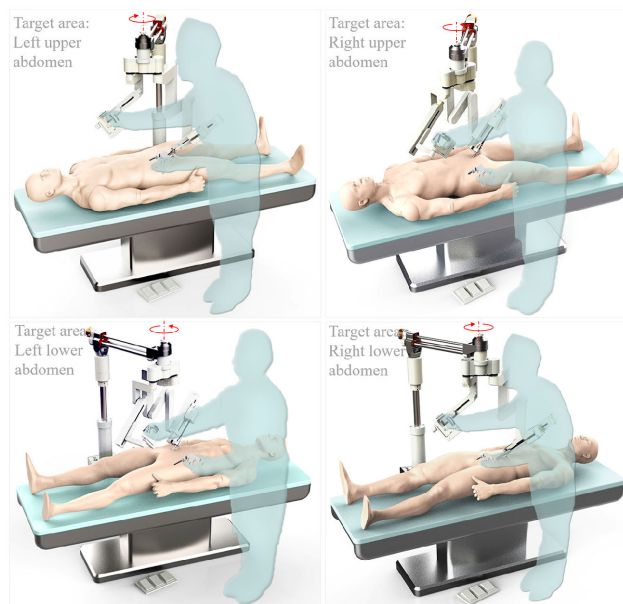
the manipulators. This master-slave integrated, table-based structural design greatly reduces the size and weight of the robot.

A swivel head on which the master and slave manipulators are mounted is designed at the tip of the crossbeam. This swivel head can be manually rotated from $-90°$ to $90°$, as shown in Fig. 3. Moreover, this device fulfills the various operation postures in different operations. By adjusting the position and direction of the swivel head, the manipulators can quickly reach the initial surgical positions during the preoperative procedure.

The master manipulator of the robot is used to acquire motion information of the surgeon's hand, whereas the slave manipulator is used to manipulate the multi-DOF instrument. To meet the requirements of incision constraints, the instrument of the robot should pivot around the incision, which requires the slave manipulator to realize a specific kinematic movement; this pivot point is the remote center of motion (RCM). The proposed surgical robot adopts a mechanical self-restraint mechanism to realize an RCM. The slave manipulator of the robot is designed based on a double parallelogram mechanism, as shown in Fig. 4, and a cable transmission method is adopted in the mechanical design of the slave manipulator to reduce volume and weight and to avoid the singularity that exists in link-based parallelogram structures.

The workspace of MIS robots should be able to meet the needs of minimally invasive surgery. For surgical instruments to reach any surgical field in the abdominal cavity, the surgical instruments need to be able to pitch by $160°$ and yaw by $120°$ around the RCM point [32]. By reasonably selecting the access location of the robot, the workspace of MIS robots can cover the volume of the abdominal cavity
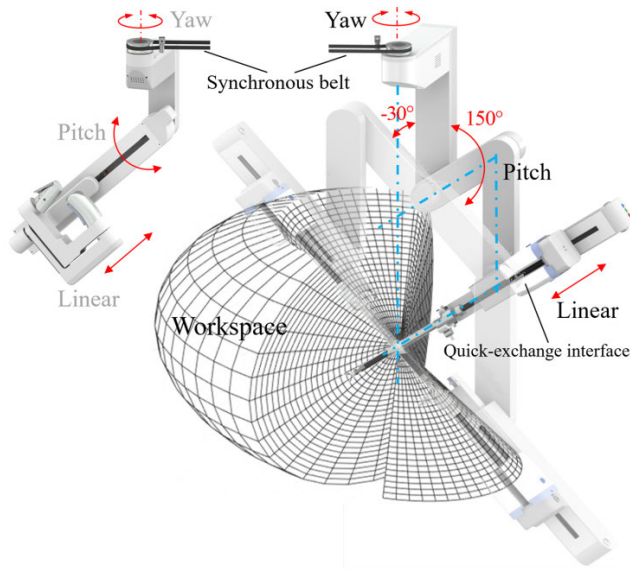
**IEEE** *Access*

H. Zhang *et al.*: System Design of a Novel MIS Robot That Combines the Advantages of MIS Techniques and Robotic Technology



**FIGURE 4.** Master and slave manipulators of the MIS robot.



**FIGURE 5.** Structure of the quick-exchange interface.



**FIGURE 6.** Schematic diagram of surgical instrument manipulation for suturing.

to meet surgical requirements. However, without increasing the volume of the robot, the workspace is preferably as large as possible to allow the robot to adapt to different complex situations. For the proposed MIS robot, folding and unfolding the slave manipulator can realize the pitch motion of the instrument shaft. Due to the folding joint layout, the pitch motion can reach a range of −30° to 150°. To further realize the RCM, the rotation axis of the slave manipulator relative to the swivel head passes through the RCM of the double parallelogram mechanism, and the corresponding rotation motion realizes the yaw motion (−75° to 75°) of the instrument shaft. Therefore, the workspace of the proposed robot can cover the volume of the abdominal cavity. In addition, because a complex operation often requires a variety of instruments, quick-exchange functionality is indispensable. Thus, a quick-exchange interface is designed at the distal end of the slave manipulator, and the translation of the quick-exchange interface realizes the linear motion of the instruments with a range of 0-260 mm. To simplify the kinematic control algorithm, the master manipulator, which functions as the motion input device of the robot, adopts the same DOF layout as the slave manipulator; that is, the master manipulator also has pitch, yaw, and linear DOFs. Moreover, the rotating joints of the master and slave manipulators relative to the swivel head are directly connected with a synchronous belt, as shown in Fig. 4.

Depending on the clinical requirements, instruments that have been sterilized before operation should be kept sterile during surgery. Therefore, an aseptic isolation adapter is designed between the quick-exchange interface and the instruments, as shown in Fig. 5. Moreover, the driving system of the instruments is also highly integrated into the quick-exchange interface to further reduce the size and complexity of the robot.

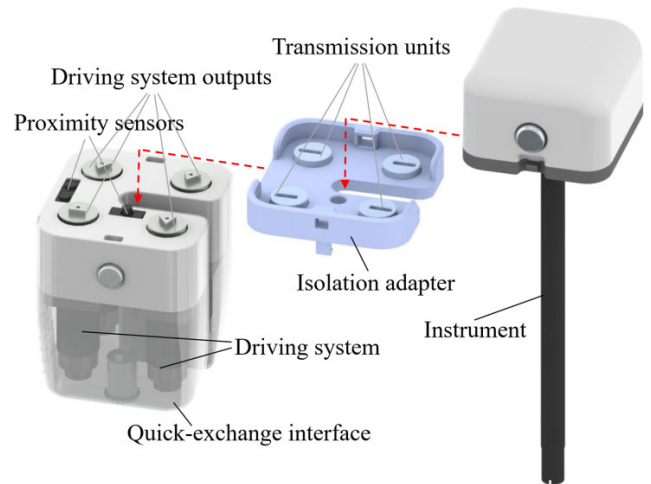A novel instrument is designed for the robot to reduce the difficulty of surgical operations. Suturing is one of the most important and complex surgical operations. In a suture operation, the movement of the needle is roughly a rotation about the bisector line of the two jaws of the instrument. The da Vinci surgical system, in which the instrument has a roll-pitch-yaw DOF arrangement, realizes the suture motion by using six-axis coordinated motion. This demands a complicated control algorithm and high overall system requirements. To complete the suturing action more simply and effectively, a roll joint rotating about its own axis is designed at the distal end of the instrument, so that the novel instrument has a roll-pitch-distal roll DOF arrangement. Under this condition, by combining the movements of the slave manipulator, the proposed surgical robot executes 7-DOF motion, as shown in Fig. 6. During surgery, when the axis of the distal roll joint is adjusted parallel to the incision direction of the tissue, the suturing action can be easily achieved by rotating only the distal roll joint.
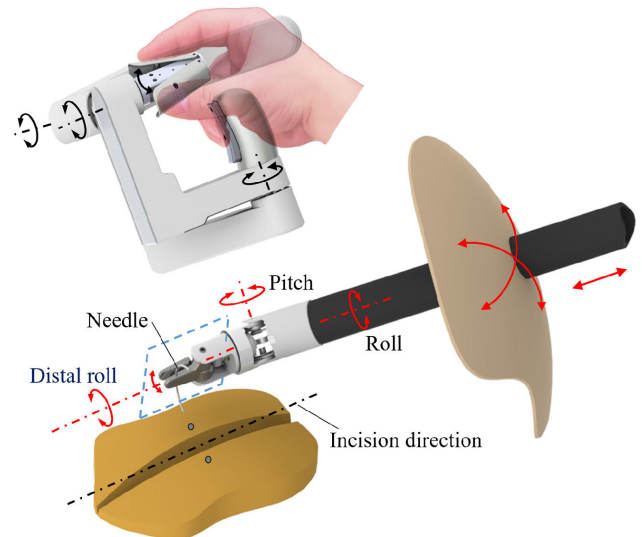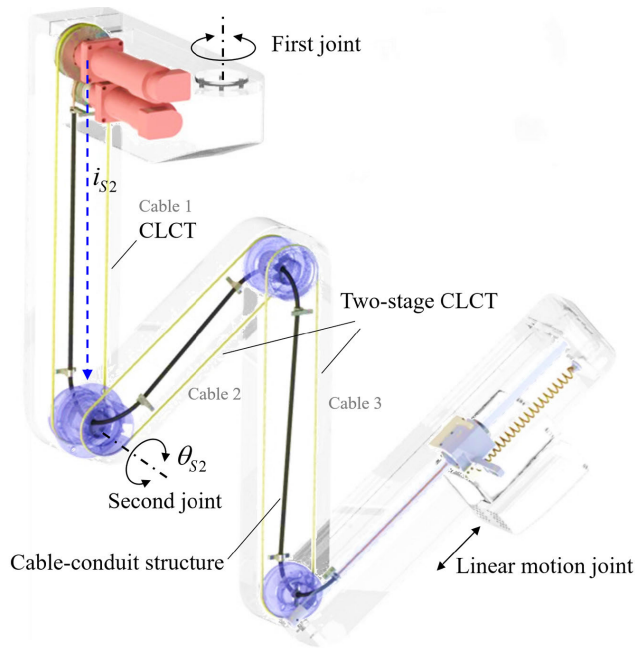
H. Zhang *et al.*: System Design of a Novel MIS Robot That Combines the Advantages of MIS Techniques and Robotic Technology

**IEEE** *Access*



**FIGURE 7.** Multistage cable transmission structure of the slave manipulator.

To intuitively enhance the manipulability, the handle of the master manipulator adopts the same DOF arrangement as the instrument, as shown in Fig. 6. The ergonomic design of the holding structure enables the handle to match a human hand very well. In particular, the motion of the distal roll joint of the handle is very similar to the twisting motion of the thumb and forefinger and thus can fully exploit the flexibility of the operator's hand.

## III. TRANSMISSION MODEL OF THE ROBOT

A reasonable transmission structure and accurate transmission model are essential for an MIS robot to precisely perform operations. In robot-assisted minimally invasive surgery, the motion information of the master manipulator of the proposed robot is measured with sensors and encoders, which are mounted directly at each joint of the master manipulator. Therefore, only the transmission structure of the slave manipulator needs to be analyzed. For the slave manipulator of the proposed MIS robot, due to the size limitation of the mechanical structure, a cable transmission method is adopted to achieve long-distance power transmission in the confined space, as shown in Fig. 7.

The first joint of the slave manipulator is directly connected to the first joint of the master manipulator through a typical synchronous belt rather than by means of a control method, which helps reduce the complexity of the control system. A two-stage closed-loop cable transmission (CLCT) structure based on the double parallelogram principle is designed to realize the RCM of the slave manipulator, whereas a CLCT is used to realize the motor postposition of the second joint. By contrast, because the remaining space within the linear motion joint is too narrow for the closed-loop cables
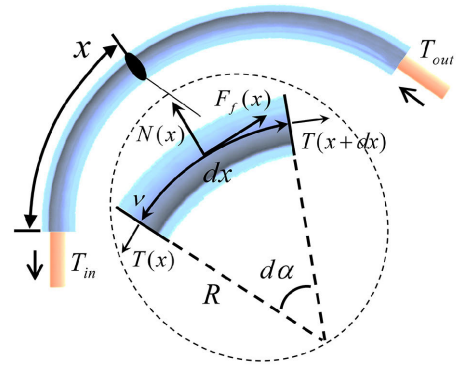


**FIGURE 8.** Force analysis model of a random element in the cable-conduit structure.

to convolve, the CLCT form is not suitable for this joint. Under this circumstance, an open-loop cable-conduit transmission structure is designed.

The next step after the design of the transmission structure is transmission modeling. Based on the structural size constraints and mechanical properties of the cable, the three CLCT structures use Carl Stahl stainless steel cables with a diameter of 1.59 mm and Young's modulus of 67 GPa. For this cable, the elastic elongation due to external force is very small and can be ignored. Moreover, guided by pulleys, the closed-loop cables experience rolling friction that is much smaller than the sliding friction experienced by the cable-conduit structure. Therefore, the elastic elongation of the closed-loop cables is very small and can be ignored to simplify the transmission model. The transmission model of the second joint of the slave manipulator can be written as

$$\alpha = i_{s2}\theta_{s2} \tag{1}$$

where $\alpha$ represents the rotation angle of the motor and $i_{s2}$ and $\theta_{s2}$ represent the transmission ratio and rotation angle of the second joint, respectively.

As mentioned above, the cable-conduit transmission form is adopted in the linear motion joint of the slave manipulator. Due to sliding friction between the cable and the conduit, the influence of the elastic elongation of the cable on the transmission model of the joint cannot be ignored. To accurately establish the transmission model of the cable-conduit structure, a method for calculating the elastic elongation of the cable with a multicurvature cable-conduit configuration is proposed in the paper.

### A. METHODOLOGY

The case of single curvature is first analyzed. In addition, the schematic diagram of the single-curvature cable-conduit configuration is shown in Fig. 8. Since the friction distribution is nonlinear, the force analysis can be performed on the segment first, and then the integral method is applied to calculate the output tension of the cable-conduit structure.

For the force analysis model of a random cable element, $x$ is the length from the input end of the conduit to the present

location; $N(x)$ is the normal force experienced by the tendon per unit length; $T(x)$ is the tension of the cable; $\mu$ is the friction coefficient between the cable and conduit; $F_f(x)$ is the friction; R is the bending radius of the cable; $T_{in}$ and $T_{out}$ are the input and output tension of the cable, respectively; and $v$ is the speed of the cable relative to the conduit. To simplify the model, $\mu$ is assumed to be the dynamic friction when the cable is moving along the conduit. Through the force balance equation, the normal force exerted on a random infinitesimal cable element is related to the tensions at the two ends by

$$N(x) = T(x)\sin\left(\frac{d\alpha}{2}\right) + T(x+dx)\sin\left(\frac{d\alpha}{2}\right) \approx T(x)d\alpha \tag{2}$$

In addition, for the angle $d\alpha$, we have

$$\begin{cases} d\alpha = dx/R \\ F_f(x) = \mu N(x)\,\mathrm{sgn}(v) \\ dT(x) = -F_f(x) \end{cases} \tag{3}$$

Substituting (3) into (2), we have

$$\frac{dT(x)}{dx} = -\frac{\mu}{R}T(x)\,\mathrm{sgn}(v) \tag{4}$$

Then, the following can be obtained:

$$T(x) = T_{in}e^{-\frac{\mu}{R}x\,\mathrm{sgn}(v)} \tag{5}$$

To analyze the elastic elongation of the cable under the tension $T(x)$, it is assumed that Hooke's law is always applicable in the elastic range of the cable. When compressing the cable, no force is transmitted through the cable. Note that $k_c$ and $A$ represent the Young's modulus and cross-sectional area of the tendon, respectively. Next, to calculate the elongation of the cable $\varepsilon$, $T_0$ is used as the preload force. In addition, it is assumed that the variation in the input tension is immediately transmitted to the output end.

Therefore, the elongation of the present section is

$$\frac{d\varepsilon(x)}{dx} = \frac{T(x) - T_0}{Ak_c} \tag{6}$$

$$\begin{aligned} \varepsilon(x) &= \int_0^x \frac{T(x) - T_0}{Ak_c}dx \\ &= \frac{1}{Ak_c}\int_0^x \left(T_{in}e^{-\frac{\mu}{R}x\,\mathrm{sgn}(v)} - T_0\right)dx \\ &= \frac{1}{Ak_c}\left(\eta(x) + \frac{R}{\mu}T_{in}\,\mathrm{sgn}(v) - T_0 x\right) \end{aligned} \tag{7}$$

where $\eta(x) = -\frac{R}{\mu}T_{in}\mathrm{sgn}(v)e^{-\frac{\mu}{R}x\,\mathrm{sgn}(v)} = -\frac{R}{\mu}T_{out}\,\mathrm{sgn}(v)$

The analysis result can be applied to a cable-conduit structure with a fixed bending radius. However, the shape of a cable-conduit structure is often not so simple in practice. There may be many bends with different curvature radii along the whole length of the conduit, as shown in Fig. 9. The cable-conduit structure is divided into $n(n \geq 1)$ segments, and a random segment $i$ (the length of the curve from the input end is $x_i$) has a different and constant radius of curvature $r_i$.
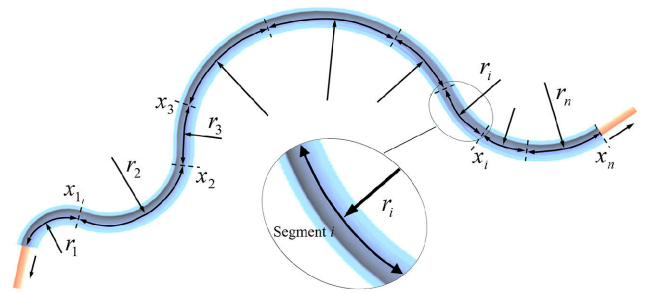


**FIGURE 9.** Multicurvature cable-conduit transmission structure.

In this case, (5) becomes

$$\begin{cases} T(x) = T_{in}\,e^{-\frac{\mu}{r1}x\,\mathrm{sgn}(v)} & (0 < x \leq x_1) \\ T(x) = T_{in}\,e^{-\frac{\mu}{r1}x_1\mathrm{sgn}(v)}e^{-\frac{\mu}{r2}(x-x_1)\,\mathrm{sgn}(v)} \\ \quad = T_{in}\,e^{-\left[\frac{1}{r1}x_1 + \frac{1}{r2}(x-x_1)\right]\mu\,\mathrm{sgn}(v)} & (x_1 < x \leq x_2) \\ T(x) = T_{in}\,e^{-\frac{\mu}{r1}x_1\mathrm{sgn}(v)}e^{-\frac{\mu}{r2}(x_2-x_1)\,\mathrm{sgn}(v)} \\ \quad \dots e^{-\frac{\mu}{rn}(x-x_{n-1})\,\mathrm{sgn}(v)} \\ \quad = T_{in}\,e^{\phi(x)} & (x_{n-1} < x \leq x_n) \end{cases} \tag{8}$$

where $\phi(x) = -\mu sgn(v)\left[\sum_{i=1}^{n-1}(x_i - x_{i-1})/r_i + (x - x_{n-1})/r_n\right]$.

By using the method of integral summation, the elastic elongation of the multicurvature cable-conduit configuration can be calculated. Thus, with (7) and (8), the elongation $\varepsilon(x_n)$ can be obtained as

$$\varepsilon(x_n) = \frac{T_{in}\,\mathrm{sgn}(v)}{Ak_c\mu}\varphi(x_n) - \frac{T_0}{Ak_c}x_n \tag{9}$$

where $\varphi(x_n) = \sum_{j=2}^{n}r_j e^{-\mu\mathrm{sgn}(v)\sum_{k=1}^{j-1}\frac{1}{r_k}(x_k-x_{k-1})}$ $(1 - e^{-\frac{\mu}{r_j}(x_j-x_{j-1})\mathrm{sgn}(v)}) + r_1(1 - e^{-\frac{\mu}{r1}x_1\,\mathrm{sgn}(v)})$.

In practical applications, the materials and preload of the cable-conduit transmission structure should be set first. Accordingly, once the shape of the cable-conduit structure is reasonably laid out and fixed, the factor $\varphi(x_n)$ becomes a fixed value. Through calibration and measurement, the curvature radius $r_i(i = 1, 2, \dots, n)$ and length $x_i(i = 1, 2, \dots, n)$ of each bending segment of the conduit can be obtained, through which the values of the factor $\varphi(x_n)$ can be determined. Then, the elongation $\varepsilon(x_n)$ can be calculated with (9).

Note that the Coulomb friction model is used in the force analysis of the cable-conduit structure. However, in practical applications, if there is a viscous lubrication medium between the cable and the conduit or the two materials have viscous properties in their mutual motion, a viscous friction model needs to be introduced. If the friction resistance between the cable and the conduit is too large, when one end of the cable moves, the other end of the cable may exhibit delayed motion. In this case, a static friction model should be introduced on the basis of the Coulomb friction model.
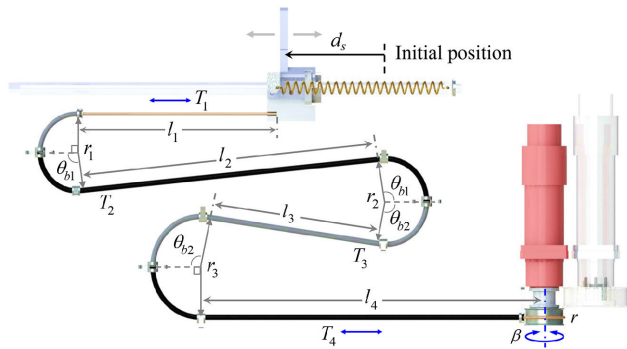
H. Zhang *et al.*: System Design of a Novel MIS Robot That Combines the Advantages of MIS Techniques and Robotic Technology

**IEEE** *Access*

**FIGURE 10. Cable-conduit transmission structure of the linear motion joint.**



**FIGURE 11. Cable transmission schematic of the surgical instrument.**

To meet the basic requirements of medical safety and reliability, viscous lubricants are prohibited in the cable-conduit transmission structure of the MIS robot, and the friction coefficient between the cable and conduit should be small. Therefore, the Coulomb friction model is adequate for the force analysis of the cable-conduit transmission structure of an MIS robot.

### B. MODELING OF THE CABLE-CONDUIT STRUCTURE

To match the mechanical structure of the slave manipulator, six bends $b_i(i = 1, 2, \ldots, 6)$ are designed in the cable-conduit transmission structure of the linear motion joint, as shown in Fig. 10, and the radii of the bends at each link joint are equal, that is, $R_{b1} = R_{b2} = r_1$, $R_{b3} = R_{b4} = r_2$, $R_{b5} = R_{b6} = r_3$. Therefore, there are actually three curvature radii $r_j(j = 1, 2, 3)$ in the cable-conduit configuration. When the motor rotates forward ($v > 0$), the force exerted by the motor on the cable makes the instrument move in, whereas when the motor rotates backward ($v < 0$), the recoil of the extension spring makes the instrument move out.

According to (8), the tensions of different cable segments $T_1 \sim T_4$ can be obtained as

$$
\begin{cases}
T_1 = T_0 + kd_s \\
T_2 = T_1 e^{-(\theta_{b1}+\pi/2)\mu \, \mathrm{sgn}(v)} \\
T_3 = T_1 e^{-(2\theta_{b1}+\theta_{b2}+\pi/2)\mu \, \mathrm{sgn}(v)} \\
T_4 = T_1 e^{-(2\theta_{b1}+2\theta_{b2}+\pi)\mu \, \mathrm{sgn}(v)}
\end{cases}
\tag{10}
$$

where $k$ is the spring coefficient of the extension spring and $d_s$ is the linear displacement of the instrument.

Then, with (9) and (10), the elongation of the cable at the bends $\varepsilon(l_b)$ can be calculated as

$$
\varepsilon(l_b) = \frac{(T_0 + kd_s)\,\mathrm{sgn}(v)}{Ak_c\mu}\varphi(l_b) - \frac{T_0}{Ak_c}l_b
\tag{11}
$$

where

$$
\begin{aligned}
\varphi(l_b) = \ & r_3 e^{-(2\theta_{b1}+\theta_{b2}+\pi/2)\mu sgn(v)}(1 - e^{-(\theta_{b2}+\pi/2)\mu sgn(v)}) \\
& + r_2 e^{-(\theta_{b1}+\pi/2)\mu sgn(v)}(1 - e^{-(\theta_{b1}+\theta_{b2})\mu sgn(v)}) \\
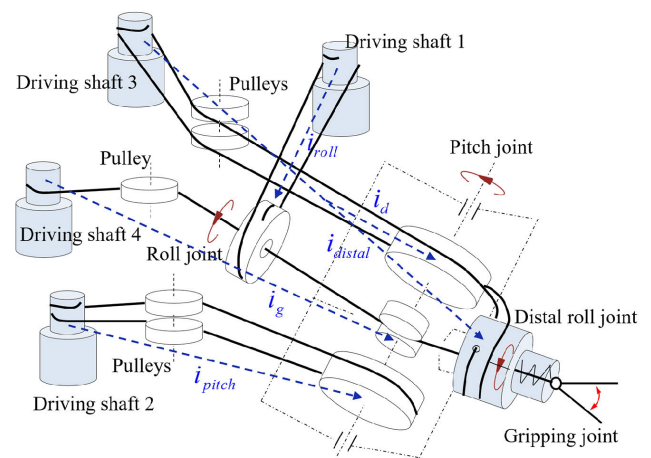& + r_1(1 - e^{-(\theta_{b1}+\pi/2)\mu sgn(v)})
\end{aligned}
$$

and

$$
l_b = (\theta_{b1} + \pi/2)r_1 + (\theta_{b1} + \theta_{b2})r_2 + (\theta_{b2} + \pi/2),
$$

which is the total length of the six bends.

In accordance with Hooke's law, the elongation of the remaining straight segments of the cable $\lambda(l_s)$ can be calculated as

$$
\lambda(l_s) = \sum_{m=1}^{4}\frac{T_m l_m}{Ak_c} - \frac{T_0}{Ak_c}l_s = \frac{(T_0 + kd_s)}{Ak_c}\psi(l_s) - \frac{T_0}{Ak_c}l_s
\tag{12}
$$

where

$$
\begin{aligned}
\psi(l_s) = \ & l_1 + l_2 e^{-(\theta_{b1}+\pi/2)\mu sgn(v)} + l_3 e^{-(2\theta_{b1}+\theta_{b2}+\pi/2)\mu sgn(v)} \\
& + l_4 e^{-(2\theta_{b1}+2\theta_{b2}+\pi)\mu sgn(v)}
\end{aligned}
$$

and

$$
l_s = \sum_{j=1}^{4} l_j,
$$

which is the total length of the straight segments of the cable.

The total elastic elongation of the cable $l_{te}$ can be written as

$$
l_{te} = \varepsilon(l_b) + \lambda(l_s)
\tag{13}
$$

where $l_{te}$ is the transmission compensation of the cable-conduit structure. Thus, the transmission model of the linear motion joint of the slave manipulator is

$$
\beta = (d_s + l_{te})/r
\tag{14}
$$

where $\beta$ and $r$ represent the rotation angle and output shaft radius of the driving motor, respectively.

As mentioned above, the wrist of the instrument has a "roll-pitch-distal roll" DOF layout. To produce a compact, lightweight design for the proposed instrument, the power transmission of each joint of the instrument is realized via cable transmission, as shown in Fig. 11. Due to the narrow
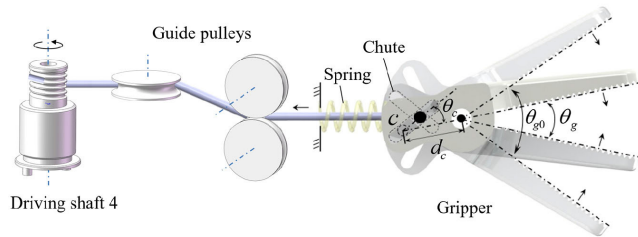
**FIGURE 12.** Transmission structure schematic of the gripping joint.



**FIGURE 13.** Motion mapping principle between the active arms of the master and slave manipulators.

space at the distal end of the instrument, all of the cables used in the instrument are Carl Stahl stainless steel cables with a Young's modulus of 67 GPa and a diameter of 0.686 mm. The CLCT structure is used in all three joints of the wrist. However, to avoid entanglement between cables, an open-loop cable transmission structure is adopted for the gripping joint. To avoid the effect of friction on the elastic elongation of cables, the transmission cables of all joints of the instruments are guided by pulleys. In addition, during surgery, the operating force generally does not exceed 20 N [33]. Depending on the structure and size of the instrument, the length of the longest cable used in the instrument is approximately 490 mm. Hence, according to (6), the maximum elastic deformation of cables in the instrument is approximately 0.04 mm, which can be ignored. Thus, the elastic elongation of the cables is ignored to simplify the transmission model.

Through structural analysis, the transmission model of the wrist of the instrument can be written as

$$
\begin{cases}
\gamma_1 = i_{roll}\theta_r \\
\gamma_2 = i_{pitch}\theta_p \\
\gamma_3 = i_{distal}\theta_d + i_d\theta_p
\end{cases}
\tag{15}
$$

where $\gamma_1$, $\gamma_2$, and $\gamma_3$ are the rotation angles of driving shafts 1, 2, and 3, respectively, whereas $\theta_r$, $\theta_p$, and $\theta_d$ are the rotation angles of roll, pitch, and the distal roll joint, respectively. Note that $i_{roll}$, $i_{pitch}$, and $i_{distal}$ are the drive ratios of the three wrist joints, the value of each drive ratio is equal to the diameter ratio of the corresponding joint shaft and driving shaft. Moreover, $i_d$ represents the diameter ratio of the guide pulley of the distal roll joint to driving shaft 3.

The gripping motion of the gripper is realized with a chute structure, as shown in Fig. 12. By structural analysis of the gripper, the transmission model of the gripper can be obtained as

$$
\gamma_4 = \left[ d_c \sin\theta_c (\sin(\theta_c + \tfrac{\theta_g}{2})^{-1} - \sin(\theta_c + \tfrac{\theta_{g0}}{2})^{-1}) \right] \Big/ r_{s4} + i_g |\theta_p| \tag{16}
$$

where $\gamma_4$ and $r_{s4}$ are the rotation angle and radius of driving shaft 4, respectively; $d_c$ and $\theta_c$ are the geometric parameters of the chute; $\theta_{g0}$ and $\theta_g$ are the initial and current opening angles, respectively; and $i_g$ represents the diameter ratio of the guide pulley of the gripping joint to driving shaft 4.
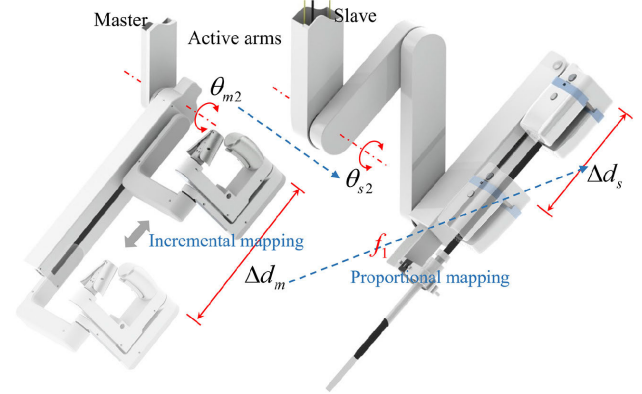
Synthesizing the above transmission analysis, the combination of (1) and (14) is the transmission model of an active arm of the slave manipulator, and the combination of (15) and (16) constitutes a transmission model of the instrument. Therefore, the combination of the above four equations constitutes the transmission model of the slave manipulator of the proposed MIS robot.

## IV. MOTION MAPPING AND CONTROL STRATEGY
### A. MASTER-SLAVE MOTION MAPPING
Establishing reasonable motion mapping on the basis of a transmission model is the key to realizing effective master-slave manipulation. As previously mentioned, the active arm of the master manipulator and that of the slave manipulator have the same DOF layout, as shown in Fig. 13, and the two arms adopt a "one-to-one" driving mode to reduce the complexity of the control algorithm and structure. That is, the pitch joint angle $\theta_{s2}$ and the linear joint movement $\Delta d_s$ of the slave manipulator are controlled by the pitch joint angle $\theta_{m2}$ and the linear joint movement $\Delta d_m$ of the master manipulator, respectively. In addition, considering that different surgical operations have different requirements for the speed of instrument movements in and out, a proportional mapping strategy is introduced into the master-slave motion mapping of the linear joints. On this basis, to avoid an inadequate motion range of the linear joint of the master manipulator, an incremental mapping strategy is introduced.

The mapping model between the active arms of the master and slave manipulators can be described as

$$
\begin{cases}
\theta_{s2} = \theta_{m2} \\
\Delta d_s = f_1 \cdot \Delta d_m
\end{cases}
\tag{17}
$$

where $f_1$ is the mapping scale factor of linear joint movement.

By introducing a scale factor $f_1$ into the mapping equation, the displacement between the linear joints of the master and slave manipulators has a fixed proportion in a mapping period. A proportional mapping strategy is always used to convert the large movement of the master manipulator into the small movement of the slave manipulator; thus, $0 < f_1 \leq 1$. This strategy is helpful to improve operation accuracy,
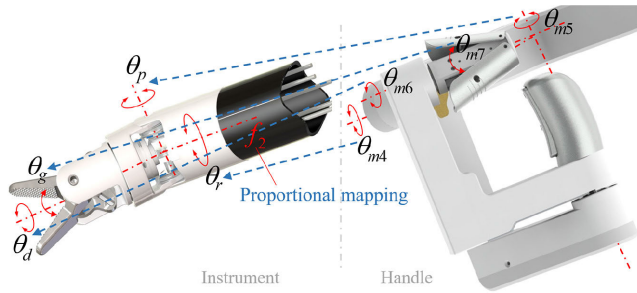
H. Zhang *et al.*: System Design of a Novel MIS Robot That Combines the Advantages of MIS Techniques and Robotic Technology

**IEEE** *Access*



**FIGURE 14.** Motion mapping principle between the handle and the instrument.



**FIGURE 15.** Control flow of master-slave mapping for the MIS robot.

especially in fine operations or hazardous situations. An incremental mapping strategy is used to reposition the handle of the master manipulator while keeping the slave manipulator still during the surgery.

Similar to the motion mapping principle between the active arms of the master and slave manipulators, the handle of the master manipulator adopts the same DOF layout as the end of the instrument. In addition, as shown in Fig. 14, the driving model is also a "one-to-one" form, i.e., the roll angle $\theta_r$, pitch angle $\theta_p$, distal roll angle $\theta_d$ and gripper opening angle $\theta_g$ of the instrument are controlled by the roll angle $\theta_{m4}$, pitch angle $\theta_{m5}$, distal roll angle $\theta_{m6}$ and opening angle $\theta_{m7}$ of the handle, respectively. Because the motion range of human fingers is limited, to maximize the advantage of the distal roll DOF, a proportional mapping strategy is introduced into the motion mapping between the distal roll joints of the handle and instrument. The mapping model between the handle and instrument can be described as

$$\begin{cases} \theta_r = \theta_{m4} \\ \theta_p = \theta_{m5} \\ \theta_d = f_2 \cdot \theta_{m6} \\ \theta_g = \theta_{m7} \end{cases} \tag{18}$$

where $f_2$ is the mapping scale factor of the distal roll movement. Note that the proportional mapping strategy for distal roll joints is used to convert the small movement of the handle into the large movement of the instrument considering the actual operation requirement; thus, $1 \leq f_2 \leq 2$.

The combination of (17) and (18) is the motion mapping model of the proposed surgical robot. In addition, the master-slave control flow of the surgical robot can be constructed as shown in Fig. 15. First, the joint information of the master manipulator is collected with the joint information acquisition module, and then the rotation angle of all the driving motors of the slave manipulator can be calculated by the established motion mapping model and transmission model. Finally, the slave manipulator follows the controller commands to perform various surgical actions.

### B. QUICK-EXCHANGE CONTROL STRATEGY

In addition to the motion mapping strategy, the quick-exchange strategy is a key control strategy of the control system. As previously mentioned, because complex operations
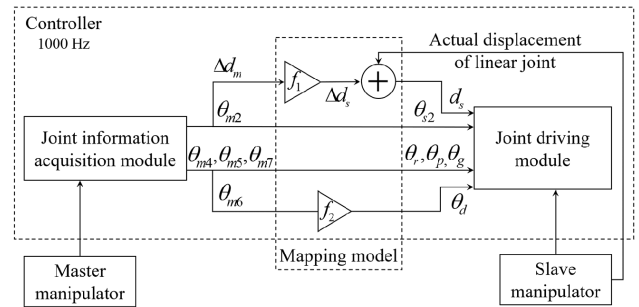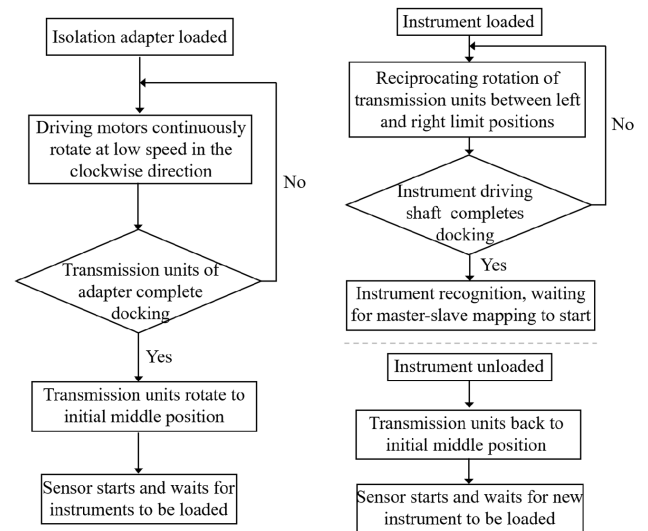


**FIGURE 16.** Block diagram of the quick-exchange procedures of the MIS robot.

often require a variety of instruments, the surgical robot requires an efficient and intelligent instrument exchange function. Due to the existence of aseptic isolation adapters, the complete instrument exchange process consists of two parts: installation of an isolation adapter and quick exchange of instruments. A block diagram of the quick-exchange procedures of the robot is shown in Fig. 16. The aseptic adapter needs to be installed first. When the isolation adapter is loaded, the driving motors on the quick-exchange interface will continuously rotate at low speed in the clockwise direction until the transmission of the adapter completes docking. Then, the transmission units rotate to the initial middle position, and the instrument detection sensor starts and waits for an instrument to be loaded. When an instrument is loaded, the transmission units will continue reciprocating between the left and right limit positions until the driving shafts of the instrument complete docking. Then, the instrument will be recognized by the robot and be ready for master-slave mapping. When the instrument is unloaded, the transmission units will return to the initial middle position, and the instrument detection sensor will start and wait for a new instrument.

By using the above quick-exchange strategy, the isolation adapter and the instrument can be automatically mounted on
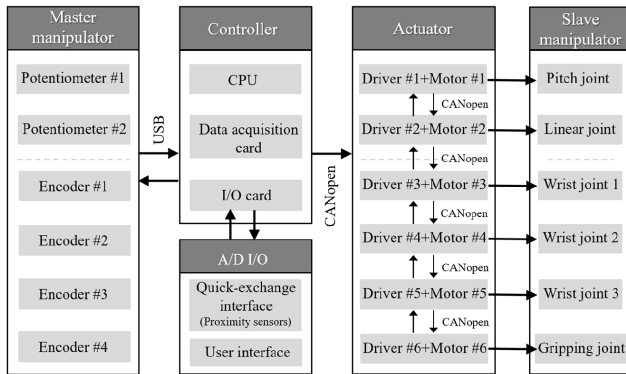
**IEEE** *Access*

H. Zhang *et al.*: System Design of a Novel MIS Robot That Combines the Advantages of MIS Techniques and Robotic Technology



**FIGURE 17.** Overall control infrastructure of the MIS robot.



**FIGURE 18.** Developed prototype of the MIS robot.

the quick-exchange interface. Note that the installation procedure for the isolation adapter only needs to be performed once before an operation, whereas the instrument exchange procedure may be performed several times during surgery as needed.

## C. CONTROL INFRASTRUCTURE

The overall control structure consists of a motion input unit, a control unit and a motion execution unit, as shown in Fig. 17. The master manipulator, as the motion input unit, is directly connected to the control unit. Two absolute position sensors (KIFEL714 potentiometer) are used to obtain the motion information of the pitch and linear joints, and four encoders (HEDL500 encoder) are used to obtain the angular information of the wrist and gripping joints. The core component of the control unit is the controller (Turbo PMAC2 controller), which is used for data and signal acquisition, analysis and processing, analog and digital I/O, control command output, etc. The motion execution unit includes 6 actuators (driver + motor) and the corresponding joints of the slave manipulator, of which two actuators (Copley ACJ-055-18 driver + Maxon RE30 motor) are used to actuate the pitch and linear joints and four actuators (EPOS2 Module36/2 driver + Maxon EC20 motor) are used to actuate the wrist and gripper.

The master manipulator and actuators are connected to the controller using USB and CANopen protocols for signal input and output control, whereas the drivers are connected using CANopen protocols. During robot-assisted minimally invasive surgery, according to the motion signals collected from the master manipulator, the controller sends control signals to the actuators, and then the slave manipulator reproduces the doctor's hand movements under the control commands.

## V. EXPERIMENTAL VERIFICATION

Based on the previously described design scheme and master-slave motion mapping strategies, a prototype of the master-slave integrated surgical robot was developed as shown in Fig. 18. Then, several experimental tasks were designed to verify the feasibility of the proposed robot and its design theories. In the experiments, the operators observed the
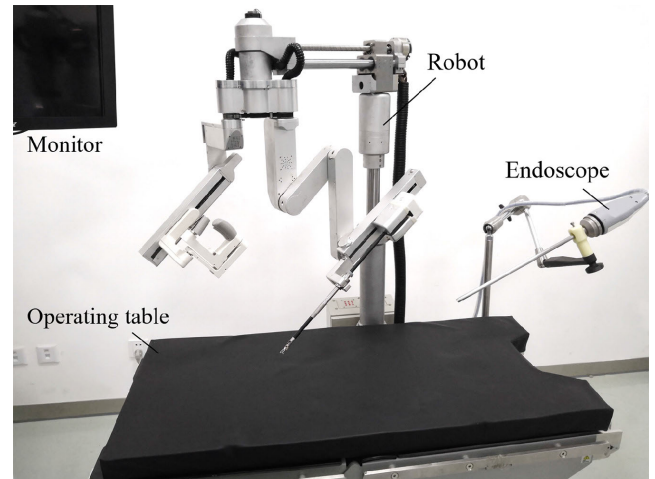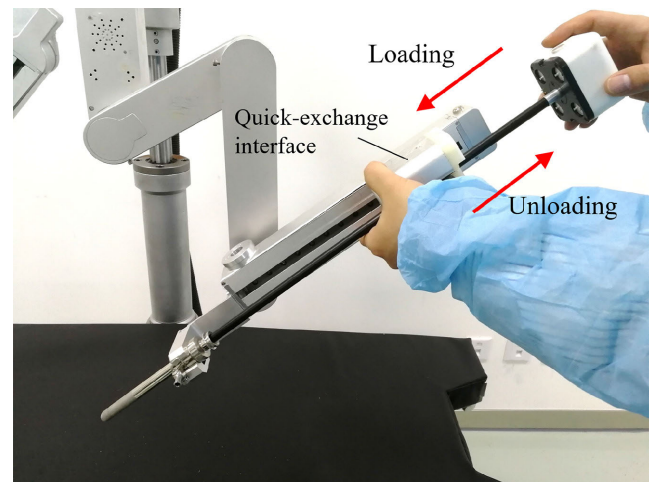


**FIGURE 19.** Quick-exchange test of the robotic instrument.

three-dimensional surgical field with a dual-eye endoscope developed by Tianjin University [34].

## A. QUICK-EXCHANGE TEST

Quick-exchange capability is one of the key performance requirements of the designed surgical robot. Accordingly, a quick-exchange test was designed for the robot as shown in Fig. 19. The complete quick-exchange procedure included instrument unloading, quick-exchange interface initialization, instrument loading, and automatic docking. Five different types of surgical instruments were used for the quick-exchange test, during which each instrument was tested 10 times; the time required for each quick-exchange procedure was recorded. The mean value of the measured times was the quick-exchange time of the robot. Then, to evaluate the completion of the quick-exchange procedure, all joints of the instrument were controlled to move after performing the quick-exchange procedure.

The measured time consumption of the quick-exchange procedure is shown in Fig. 20.
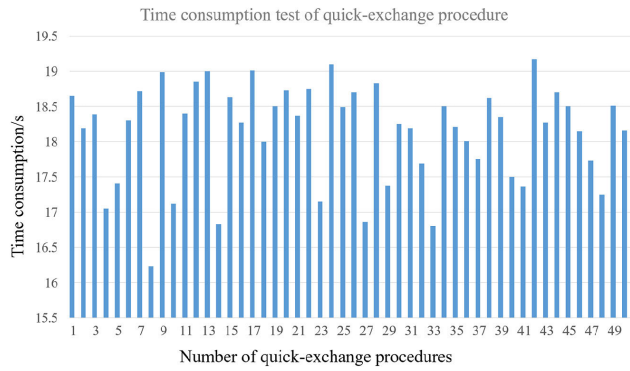
H. Zhang *et al.*: System Design of a Novel MIS Robot That Combines the Advantages of MIS Techniques and Robotic Technology

**IEEE** *Access*



**FIGURE 20.** Measured time consumption of the quick-exchange procedure.

**TABLE 1.** Quick-exchange procedure times for various surgical instruments.

| Type | Needle holder | Tissue forceps | Electric hook | Bowel clamp | Suture scissors |
|------|---------------|----------------|---------------|-------------|-----------------|
| Time | $\overline{T_1} = 17.64$ s | $\overline{T_2} = 18.05$ s | $\overline{T_3} = 18.31$ s | $\overline{T_4} = 17.86$ s | $\overline{T_5} = 17.92$ s |

The quick-exchange times of five different types of surgical instruments were calculated and are shown in Table 1.

The mean and standard deviation of the total measured data are

$$\overline{T} = 17.96 \text{ s and } S = 0.59 \text{ s} \qquad (19)$$

where $\overline{T}$ represents the quick-exchange time of the robot. The measured and calculated data show that during robot-assisted minimally invasive surgery, the quick-exchange procedure can be completed in a very short time (generally less than 20 s). As previously mentioned, all joints of the surgical instrument were controlled to move after performing each quick-exchange procedure. No docking failures occurred during these tests, meaning that the success rate of 50 quick-exchange procedures was 100%. The above test results verified the feasibility and reliability of the quick-exchange function design of the robot. Note that because the loading and unloading of the instrument must be manually performed, the quick-exchange time may be affected to some extent by the operator's proficiency. Therefore, in practice, basic operational training is required for surgeons.

## B. MAPPING MODEL VALIDATION AND ANALYSIS

To verify the effectiveness of the proposed surgical robot and its motion mapping strategy, a ring-rod test, also known as a pick-and-place test, was designed and carried out. This test, which is similar to the Hanoi tower game, can illustrate the flexibility and motion mapping accuracy of a robot. As illustrated by the test scene in Fig. 21, the operator manipulated the surgical instrument to pick up the ring, adjusted the posture of the end of the instrument to make the ring pass over the fixed rod, and finally placed the ring on the bottom of the rod. When the ring is passing over the rod, the plane
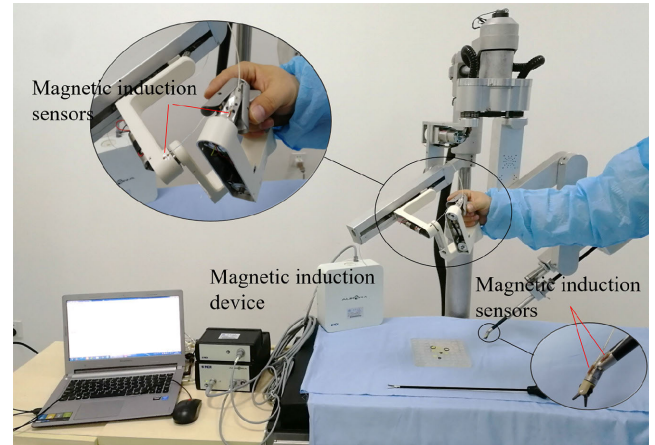


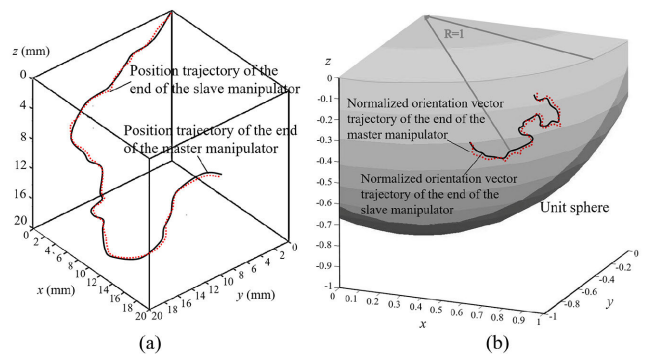**FIGURE 21.** Experimental setup of the ring-rod test for the MIS robot.



**FIGURE 22.** Position and orientation motion trajectories of the master and slave manipulators.

of the ring should always be perpendicular to the rod without any contact between the two objects.

The position and orientation trajectories of the ends of the master and slave manipulators in the ring-rod test were measured with a magnetic induction device (Ascension track-STAR, Shelburne, VT, USA). Two magnetic induction sensors were fixed on the base of the wrist of the master and slave manipulators to collect position information, while another two sensors were fixed on the axis of the distal roll joint to collect orientation information. To facilitate the comparison of the position trajectories of the master and slave manipulators, $f_1$ and $f_2$ were set to 1, and the two trajectory coordinates were described in the same coordinate system as shown in Fig. 22(a). The results showed that the two sets of position trajectories were highly consistent: the maximum trajectory error was 0.46 mm. The orientation trajectory coordinates of the master and slave manipulators were normalized first and then described in the same coordinate system, as shown in Fig. 22(b). The results showed that the changes in orientation of the ends of the master manipulator and instrument were also very consistent: the maximum trajectory error was 0.87°. These test results show that the developed surgical robot exhibits precise master-slave tracking characteristics
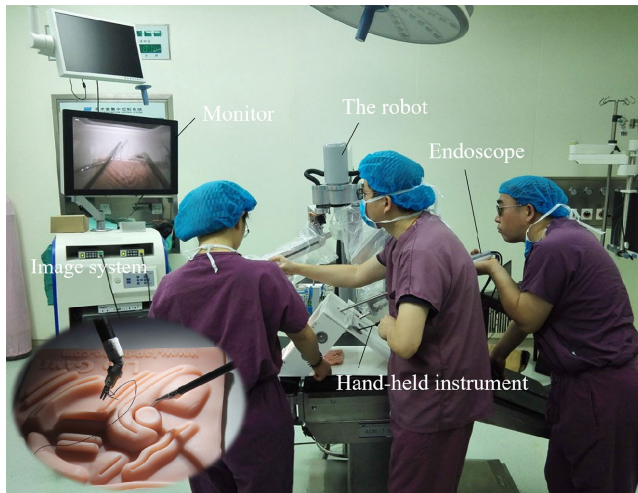
**FIGURE 23.** Simulated suture test with the MIS robot.



**FIGURE 24.** Angle changes of the wrist joints of the surgical instrument during the suture test.

and verify the feasibility of the designed robot and its motion mapping strategy.

Trajectory errors are partially caused by the uncertainty of the measurements and deviations from the transmission model. The main deviation source is the small elastic deformation of the CLCT structure of the robot; therefore, taking elastic deformation into account when modeling the CLCT structure will further improve the accuracy of master-slave motion. However, this approach will also greatly increase the complexity of the control algorithm.

### C. SUTURING CAPABILITY TEST

A simulated suture test was designed to verify the feasibility of the proposed instrument for the MIS robot and its design theory. The test is shown in Fig. 23. First, the robot was manipulated to position the instrument close to the suture area of the simulated tissue model. Then, the wrist was quickly adjusted so that the axis of the distal roll joint was parallel to the incision. Thereafter, the suture task was completed with a medical suture needle.

The simulated suture test was smoothly completed, and the suture needle penetrated the simulated tissue model in an accurate direction. The accurate position and orientation adjustments of the robot in the test not only validated the rationality of the instrument design but also preliminarily validated the feasibility of the master-slave motion mapping of the robot. Fig. 24 shows the angle changes of the four joints in the instrument. The position and orientation adjustments were carried out at 0-11 s, and the suture operation was performed at 11-19 s. The results showed that the angle of the distal roll joint changed evenly during suturing, whereas the angles of the roll and pitch joints remained approximately constant. These findings showed that under the coordination of the slave manipulator, suturing can be easily realized by mainly rotating the distal roll joint.

The test results were consistent with the design concept of the proposed instrument with a "roll-pitch-distal roll" wrist,
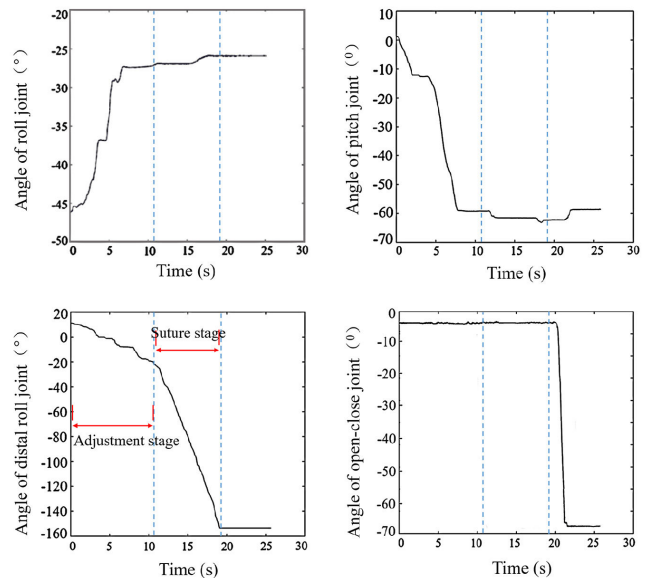
and this distal rotation needle-piercing method will help to reduce the difficulty of suture operations, thereby greatly improving the efficiency of surgery.

### D. ANIMAL EXPERIMENT

On the basis of the above tests, an animal (pig) experiment was carried out to systematically verify the feasibility and practicability of the proposed robot. A gastrointestinal anastomosis surgery was performed by three doctors (a surgeon, an assistant and an anesthetist) in a hospital animal laboratory. During the surgery, the surgeon manipulated the robot with his right hand and the handheld instrument with his left hand to perform the operation, whereas the assistant was responsible for holding the endoscope. All procedures in the operation complied with animal ethics standards, and the experimental pig was in an ideal anesthetized state during the operation.

The animal experiment scene is shown in Fig. 25. Fig. 25(a) shows the preoperative preparation procedure for the robot, Fig. 25(b) shows the trocar placement in the surgery (one trocar was for the robotic instruments, one trocar was for the handheld instruments, one trocar was for the endoscope, and the remaining trocar was reserved), Fig. 25(c) shows the surgical procedure, and Fig. 25(d) shows the various robotic instruments required for the surgery. During gastrointestinal anastomosis surgery, a series of surgical actions, including freeing, lifting, suturing, and knotting, need to be completed. As a precise, continuous suture is required along the gastric and intestinal anastomotic stomas, this surgery can effectively verify the flexibility and reliability of the developed robot, especially its ability to perform complex suture operations.

The operation scene inside the abdominal cavity is shown in Fig. 26. The colon segment to be anastomosed was pulled to the stomach by the robot with the assistance of handheld instruments. Then, the anastomotic stomas were
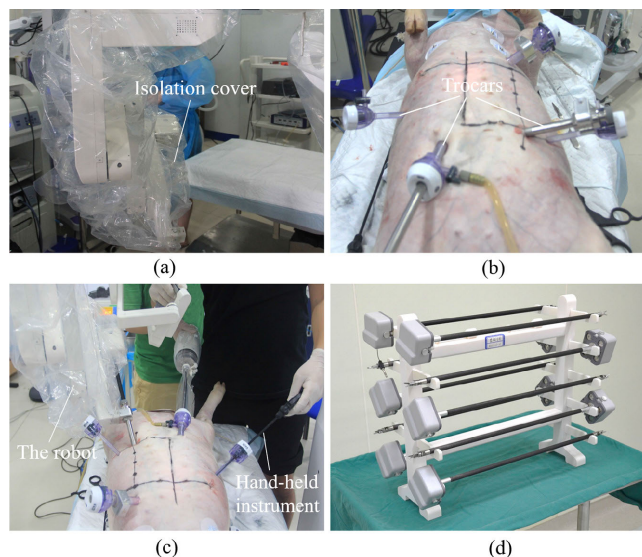
H. Zhang *et al.*: System Design of a Novel MIS Robot That Combines the Advantages of MIS Techniques and Robotic Technology

**IEEE** *Access*



**FIGURE 25.** Operation scene of the animal (pig) experiment:
(a) preoperative preparation, (b) trocar placement, (c) operation, and
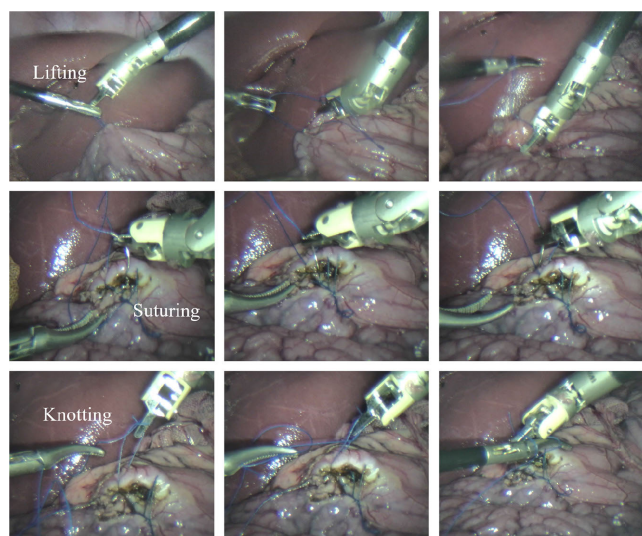(d) instruments.



**FIGURE 26.** Operation procedures of the gastrointestinal anastomosis.

selected at the proper sites of the gastric wall and intestinal segment, and a continuous suture was performed along the two anastomotic stomas with the robotic instruments. Subsequently, the knotting procedure was performed to complete the stomach-colon anastomosis operation. Finally, the gastrointestinal anastomosis surgery was successfully completed. The total operation time, including preoperative preparation, was approximately 2.5 hours. During the surgery, the complex suturing and knotting operation, which is difficult to complete with the traditional MIS technique, took only 20 minutes. In the surgery, two kinds of robotic instruments (a needle holder and an electric hook) were used, and the quick-exchange procedure was performed twice, with each procedure taking no more than 20 s.

During the surgery, the surgeon smoothly completed all desired operation tasks with the robot. According to the surgeon's feedback after the operation, the developed surgical robot can flexibly reproduce various surgical actions and perform surgical tasks as desired; moreover, the surgeon experienced an enhanced sense of intuitive motion. The experimental results presented above systematically verified the feasibility of the designed surgical robot. In addition, the statistical intraoperative blood loss in this experiment was less than 10 ml, which also reflects the accuracy and practicability of the robot.

## VI. LIMITATIONS OF THE STUDY

Although the proposed robot exhibited excellent performance during the experiment, there are still some limitations that need to be solved in future research. First, because right-handed people are far more common than left-handed people, the robot was designed for right-handed operation. Therefore, a left-handed surgeon may have difficulty operating this robot and be unable to take advantage of the flexibility of the robot. In future research, an MIS robot will be designed for left-handed operation, and the differences in the ability of left-handed and right-handed people to use the robot to complete operations will be analyzed. The corresponding research results can guide surgeons with different dominant hands to better complete surgeries with assistance from the proposed robot and expand the scope of application of surgical robots.

Second, although several experiments were designed to verify the functionality and performance of the robot, the actual surgical operation was limited to an animal experiment. In the animal experiment, the surgeon manipulated the robot to complete gastrointestinal anastomosis, which verified the feasibility of the robot. However, in future research, a greater number and additional kinds of animal experiments are needed to further verify the reliability, stability and safety of the robot and to study the scope of application of the robot.

An additional limitation of this study was that the design process of the proposed robot primarily focused on the need for minimally invasive surgery without adequate consideration of operational performance requirements. In the future, based on ergonomics research, the structure of the master manipulator and the handle can be further optimized to improve the operability of the robot and alleviate surgeon fatigue. In addition, a more reasonable interaction interface will be designed to avoid incorrect operations by surgeons during surgery. This will upgrade the comfort of operation and further improve the safety of the robot.

Finally, the study was limited by the cable transmission system, as only the elastic elongation of the open-loop cable-conduit transmission structure was considered. This approach greatly simplified the transmission model but also introduced systematic errors that reduced the performance of the robot. To increase the accuracy and reliability of the cable transmission system, future research should carry out further analyses of elastic elongation, fatigue and stress relaxation of the

**IEEE** *Access*

H. Zhang *et al.*: System Design of a Novel MIS Robot That Combines the Advantages of MIS Techniques and Robotic Technology

cable. This approach will allow the transmission error to be compensated and the control accuracy of the robot to be improved. However, despite these limitations, this study verified the feasibility and clinical potential of the robot through reasonable experiments, thereby providing a new research direction for the miniaturization of MIS robots.

## VII. CONCLUSION AND DISCUSSION

With the rapid development of robot-assisted MIS technology, miniaturization and portability have gradually become an important direction in research on MIS robots. Based on the proposed new operation mode, a new table-attached, master-slave integrated MIS robot is designed in this paper.

The proposed MIS robot combines the high efficiency of traditional MIS techniques with the dexterity of robotic operations and solves the large volume and heavy weight problems of existing master-slave MIS robots and the poor intuitive manipulability problems of existing handheld robots. Moreover, this paper proposes a "one-to-one" driving mode, which simplifies the control algorithm of the robot and improves the reliability of the control system under the premise of highly accurate motion mapping.

The proposed robot adopts a cable transmission method, and an open-loop cable-conduit transmission structure is designed to reduce the size and improve the motion performance of the robot by realizing motor postposition. Focusing on the open-loop cable-conduit transmission structure, a modeling method is proposed based on cable transmission error compensation for a multicurvature cable-conduit configuration, which improves the transmission and control accuracy.

To improve the manipulability of the robot, this paper analyzes the characteristics of the most complicated operation— suturing in minimally invasive surgery—and then designs a new surgical instrument with a "roll-pitch-distal roll" wrist to reduce the difficulty of controlling the instrument during suturing. Moreover, through an analysis of ergonomics, this paper designs a master manipulator handle that can greatly reduce the surgeon's difficulty in completing the suturing operation.

This paper also designs an intelligent quick-change interface with aseptic isolation functionality, which not only meets the sterility requirements of the operation but also enables quick changes between different types of instruments.

Finally, a series of experiments, including an animal experiment, were conducted, which fully demonstrated the feasibility and clinical potential of the proposed MIS robot.

## REFERENCES

[1] P. Gomes, "Surgical robotics: Reviewing the past, analysing the present, imagining the future," *Robot. Comput.-Integr. Manuf.*, vol. 27, no. 2, pp. 261–266, Apr. 2011, doi: 10.1016/j.rcim.2010.06.009.

[2] P. Kazanzides, G. Fichtinger, G. D. Hager, A. M. Okamura, L. L. Whitcomb, and R. H. Taylor, "Surgical and interventional robotics–core concepts, technology, and design [Tutorial]," *IEEE Robot. Autom. Mag.*, vol. 15, no. 2, pp. 122–130, Jun. 2008, doi: 10.1109/MRA.2008.926390.

[3] A. S. Naidu, R. V. Patel, and M. D. Naish, "Low-cost disposable tactile sensors for palpation in minimally invasive surgery," *IEEE/ASME Trans. Mechatronics*, vol. 22, no. 1, pp. 127–137, Feb. 2017, doi: 10.1109/TMECH.2016.2623743.

[4] A. S. Vemuri, J. C.-H. Wu, K.-C. Liu, and H.-S. Wu, "Deformable three-dimensional model architecture for interactive augmented reality in minimally invasive surgery," *Surgical Endoscopy*, vol. 26, no. 12, pp. 3655–3662, Jun. 2012, doi: 10.1007/s00464-012-2395-0.

[5] S. U. Bae, W. K. Jeong, O. S. Bae, and S. K. Baek, "Reduced-port robotic anterior resection for left-sided colon cancer using the da Vinci single-site platform," *Int. J. Med. Robot. Comput. Assist. Surgery*, vol. 12, no. 3, pp. 517–523, Jun. 2015, doi: 10.1002/rcs.1677.

[6] H. J. Lee, G.-S. Choi, J. S. Park, S. Y. Park, H. J. Kim, I. T. Woo, and I. K. Park, "A novel robotic right colectomy for colon cancer via the suprapubic approach using the da vinci xi system: Initial clinical experience," *Ann. Surgical Treatment Res.*, vol. 94, no. 2, pp. 83–87, 2018, doi: 10.4174/astr.2018.94.2.83.

[7] R. Konietschke, D. Zerbato, R. Richa, A. Tobergte, P. Poignet, F. A. Fröhlich, D. Botturi, P. Fiorini, and G. Hirzinger, "Integration of new features for telerobotic surgery into the mirosurge system," *Appl. Bionics Biomech.*, vol. 8, no. 2, pp. 253–265, 2011, doi: 10.1155/2011/635951.

[8] U. Hagn, R. Konietschke, A. Tobergte, M. Nickl, S. Jörg, B. Kübler, G. Passig, M. Gröger, F. Fröhlich, U. Seibold, L. Le-Tien, A. Albu-Schäffer, A. Nothhelfer, F. Hacker, M. Grebenstein, and G. Hirzinger, "DLR MiroSurge: A versatile system for research in endoscopic telesurgery," *Int. J. Comput. Assist. Radiol. Surgery*, vol. 5, no. 2, pp. 183–193, Jun. 2009, doi: 10.1007/s11548-009-0372-4.

[9] M. Seeber, A. Karguth, and C. Trommer, "Device for supporting and positioning of a surgical instrument and/or an endoscope for use in minimal-invasive surgery and a surgical robotic system," U.S. Patent 0 005 784, Jan. 1, 2015.

[10] D. K. Kim, D. W. Park, and K. H. Rha, "Robot-assisted partial nephrectomy with the REVO-I robot platform in porcine models," *Eur. Urol.*, vol. 69, no. 3, pp. 541–542, Mar. 2016, doi: 10.1016/j.eururo.2015.11.024.

[11] A. Abdel Raheem, I. S. Troya, D. K. Kim, S. H. Kim, P. D. Won, P. S. Joon, G. S. Hyun, and K. H. Rha, "Robot-assisted fallopian tube transection and anastomosis using the new REVO-I robotic surgical system: Feasibility in a chronic porcine model," *BJU Int.*, vol. 118, no. 4, pp. 604–609, May 2016, doi: 10.1111/bju.13517.

[12] S. H. Choi, "Surgical robot system and method for controlling surgical robot system," U.S. Patent 9 433 470, Sep. 6, 2016.

[13] S. Atallah, E. Parra-Davila, and A. G. F. Melani, "Assessment of the versius surgical robotic system for dual-field synchronous transanal total mesorectal excision (taTME) in a preclinical model: Will Tomorrow's surgical robots promise newfound options?" *Techn. Coloproctol.*, vol. 23, no. 5, pp. 471–477, May 2019, doi: 10.1007/s10151-019-01992-1.

[14] A. R. Hutchins, R. J. Manson, R. Lerebours, A. E. Farjat, M. L. Cox, B. P. Mann, and S. Zani, "Objective assessment of the early stages of the learning curve for the senhance surgical robotic system," *J. Surgical Edu.*, vol. 76, no. 1, pp. 201–214, Jan. 2019, doi: 10.1016/j.jsurg.2018.06.026.

[15] S. Gueli Alletti, C. Rossitto, S. Cianci, E. Perrone, S. Pizzacalla, G. Monterossi, G. Vizzielli, S. Gidaro, and G. Scambia, "The Senhance surgical robotic system ('Senhance') for total hysterectomy in obese patients: A pilot study," *J. Robotic Surgery*, vol. 12, no. 2, pp. 229–234, Jun. 2017, doi: 10.1007/s11701-017-0718-9.

[16] G. S. Guthart and J. K. Salisbury, "The intuitive telesurgery system: Overview and application," in *Proc. IEEE. Int. Conf. Robot. Autom.*, San Francisco, CA, USA, Apr. 2000, pp. 618–621.

[17] J. Rosen, L. N. Sekhar, D. Glozman, M. Miyasaka, J. Dosher, B. Dellon, K. S. Moe, A. Kim, L. J. Kim, T. Lendvay, Y. Li, and B. Hannaford, "Roboscope: A flexible and bendable surgical robot for single portal minimally invasive surgery," in *Proc. IEEE Int. Conf. Robot. Autom. (ICRA)*, Singapore, May 2017, pp. 2364–2370.

[18] N. Zemiti, G. Morel, T. Ortmaier, and N. Bonnet, "Mechatronic design of a new robot for force control in minimally invasive surgery," *IEEE/ASME Trans. Mechatronics*, vol. 12, no. 2, pp. 143–153, Apr. 2007, doi: 10.1109/TMECH.2007.892831.

[19] U. Kim, D.-H. Lee, Y. B. Kim, D.-Y. Seok, J. So, and H. R. Choi, "S-surge: Novel portable surgical robot with multiaxis force-sensing capability for minimally invasive surgery," *IEEE/ASME Trans. Mechatronics*, vol. 22, no. 4, pp. 1717–1727, Aug. 2017, doi: 10.1109/TMECH.2017.2696965.

H. Zhang *et al.*: System Design of a Novel MIS Robot That Combines the Advantages of MIS Techniques and Robotic Technology

IEEE *Access*

[20] M. A. Laribi, M. Arsicault, T. Riviere, and S. Zeghloul, "Toward new minimally invasive surgical robotic system," in *Proc. IEEE Int. Conf. Ind. Technol.*, Athens, Greece, Mar. 2012, pp. 504–509.

[21] J. Li, N. Zhou, S. Wang, Y. Gao, and D. Liu, "Design of an integrated master-slave robotic system for minimally invasive surgery," *Int. J. Med. Robot. Comput. Assist. Surgery*, vol. 8, no. 1, pp. 77–84, Oct. 2011, doi: 10.1002/rcs.439.

[22] J. Choi, J. W. Park, D. J. Kim, J. Shin, C. Y. Park, J. C. Lee, and Y. H. Jo, "Lapabot: A compact telesurgical robot system for minimally invasive surgery: Part I. System description," *Minimally Invasive Therapy Allied Technol.*, vol. 21, no. 3, pp. 188–194, Jul. 2011, doi: 10.3109/13645706.2011.579979.

[23] N. Matsuhira, M. Jinno, T. Miyagawa, T. Sunaoshi, T. Hato, Y. Morikawa, T. Furukawa, S. Ozawa, M. Kitajima, and K. Nakazawa, "Development of a functional model for a master–slave combined manipulator for laparoscopic surgery," *Adv. Robot.*, vol. 17, no. 6, pp. 523–539, Apr. 2012, doi: 10.1163/15685530360675523.

[24] M. A. Sieber, B. Fellmann-Fischer, and M. Mueller, "Performance of Kymerax precision-drive articulating surgical system compared to conventional laparoscopic instruments in a pelvitrainer model," *Surgical Endoscopy*, vol. 31, no. 10, pp. 4298–4308, Mar. 2017, doi: 10.1007/s00464-017-5438-8.

[25] A. Hassan-Zahraee, B. Herman, and J. Szewczyk, "Mechatronic design of a hand-held instrument with active trocar for laparoscopy," in *Proc. IEEE Int. Conf. Robot. Autom.*, Shanghai, China, May 2011, pp. 1890–1895.

[26] R. Miyazaki, K. Hirose, Y. Ishikawa, T. Kanno, and K. Kawashima, "A master–slave integrated surgical robot with active motion transformation using wrist axis," *IEEE/ASME Trans. Mechatronics*, vol. 23, no. 3, pp. 1215–1225, Jun. 2018, doi: 10.1109/TMECH.2018.2817212.

[27] M. Sholev, "Interface between user and laparoscopic tools," U.S. Patent 14 63 2061, Feb. 26, 2015.

[28] S. Awtar, T. T. Trutna, J. M. Nielsen, R. Abani, and J. Geiger, "FlexDex: A minimally invasive surgical tool with enhanced dexterity and intuitive control," *J. Med. Device*, vol. 4, no. 3, pp. 035003-1–035003-8, Sep. 2010, doi: 10.1115/1.4002234.

[29] Y.-H. Kim, Y.-J. Park, H. In, C. W. Jeong, and K.-J. Cho, "Design concept of hybrid instrument for laparoscopic surgery and its verification using scale model test," *IEEE/ASME Trans. Mechatronics*, vol. 21, no. 1, pp. 142–153, Feb. 2016, doi: 10.1109/TMECH.2015.2453321.

[30] C. J. Payne, G. Gras, M. Hughes, D. Nathwani, and G.-Z. Yang, "A hand-held flexible mechatronic device for arthroscopy," in *Proc. IEEE/RSJ Int. Conf. Intell. Robots Syst. (IROS)*, Hamburg, Germany, Sep. 2015, pp. 817–823.

[31] Y. Yang, K. Kong, J. Li, S. Wang, and J. Li, "Design and evaluation of a dexterous and modular hand-held surgical robot for minimally invasive surgery," *J. Med. Devices*, vol. 13, no. 4, Oct. 2019, Art. no. 041005, doi: 10.1115/1.4044527.

[32] A. J. Madhani, G. Niemeyer, and J. K. Salisbury, "The black falcon: A teleoperated surgical instrument for minimally invasive surgery," in *Proc. IEEE/RSJ Int. Conf. Intell. Robots Syst. Innov. Theory, Pract. Appl.*, Victoria, BC, Canada, vol. 2, Oct. 1998, pp. 936–944.

[33] P. Mucksavage, D. C. Kerbl, D. L. Pick, J. Y. Lee, E. M. McDougall, and M. K. Louie, "Differences in grip forces among various robotic instruments and da vinci surgical platforms," *J. Endourology*, vol. 25, no. 3, pp. 523–528, Mar. 2011, doi: 10.1089/end.2010.0306.

[34] H. Su, J. Li, K. Kong, and J. Li, "Development and experiment of the Internet-based telesurgery with MicroHand robot," *Adv. Mech. Eng.*, vol. 10, no. 2, Feb. 2018, Art. no. 168781401876192, doi: 10.1177/1687814018761921.
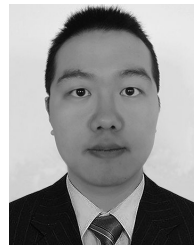
**HUAIFENG ZHANG** received the B.S. degree in mechanical engineering from Tianjin University, in 2013, where he is currently pursuing the Ph.D. degree in mechanical engineering.

He has been with the Key Laboratory of Mechanism Theory and Equipment Design of Ministry of Education, Tianjin University, since 2013. His research interests include designing dexterous robotic arms, kinematic and dynamic behavior analyses of minimally invasive surgical robots, and ergonomics.

**JIANMIN LI** (Member, IEEE) received the B.S. and Ph.D. degrees from Tianjin University, in 2006 and 2010, respectively.

From 2010 to 2012, he was a Postdoctoral Researcher with Tianjin University, where he is currently an Associate Professor with the Department of Mechanical Engineering. His research interests include mechanical design, kinematics, and motion mapping strategies for minimally invasive surgical robots, multifunctional surgical instruments, and dynamic modeling of cable-driven systems.
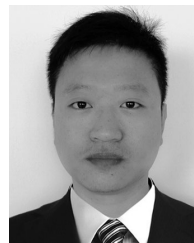
**KANG KONG** received the M.S. and Ph.D. degrees in mechanical engineering from Tianjin University, in 2012 and 2017, respectively.

He is currently a Lecturer with the Department of Mechanical Engineering, Tianjin University, where he is also working with the Key Laboratory of Mechanism Theory and Equipment Design of Ministry of Education. His research interests include mechanism design and analysis of minimally invasive surgical robots, dexterous robotic arms, and automatic control.

**SHUXIN WANG** (Member, IEEE) received the M.S. and Ph.D. degrees in mechanical engineering from Tianjin University, in 1990 and 1994, respectively.

From 1994 to 1998, he was an Associate Professor with Tianjin University, where he is currently a Professor with the Department of Mechanical Engineering. Since 2009, he has been serving as the Director of the Key Laboratory of Mechanism Theory and Equipment Design of Ministry of Education, Tianjin University, where he is also responsible for research projects in the area of medical robotic systems. He has authored more than 80 technical publications. His research interests include mechanical design and the theory, development and application of surgical, and rehabilitative robot systems.

• • •